Pol. J. Environ. Stud. Vol. XX, No. X (XXXX), 1-18
DOI: *10.15244/pjoes/218653* ONLINE PUBLICATION DATE: 2026-06-03

Original Research

Novel Composites Based on Yeast-Activated Carbon, Silica, and Alginate for Removal of Phenol from Aqueous Medium: Kinetic Study

Slobodanka Stanojević-Nikolić[1], Milan P. Nikolić[1]°*, Vladimir Pavlović[2], Vladislav Rac[2], Vladimir V. Srdić[3], Marina Šćiban[3]

[1]University of Kragujevac, Faculty of Agronomy Čačak, Laboratory for Technological Processes Control and Sustainable Development, Čačak, Serbia
[2]University of Belgrade, Faculty of Agriculture, Belgrade, Serbia
[3]University of Novi Sad, Faculty of Technology Novi Sad, Novi Sad, Serbia

Received: 29 October 2025
Accepted: 27 February 2026

Abstract

In the present study, the adsorption of phenol from aqueous solution was performed by using activated carbons obtained from the pyrolysis of *S. cerevisiae* biomass and new composites obtained by immobilization of activated carbon in an alginate and silica-alginate support. The properties of adsorbents were tested by removing phenol from water in a batch process. The effects of contact time, number of adsorption cycles, and leaching of organic matter from composites were studied. The efficiency of phenol removal using activated carbons increased with the rise of activation temperature, ranging from 92.4% to 97.1%. The immobilization of activated carbon into silica-alginate gel has significant advantages compared to its immobilization into silica or alginate gel. The microstructure of the silica-alginate-activated carbon composite is strongly influenced by the alginate-silica weight ratio, resulting in different phenol removal kinetics and saturation capacities. The kinetics of the adsorption process were found to follow the pseudo-second-order kinetic model. The utilization of an alginate-activated carbon composite or a silica-alginate-activated carbon composite (the latter with an alginate-silica weight ratio of 2:1) resulted in external diffusion limitations.

Keywords: *S. cerevisiae* biomass, activated carbon, composites, phenol, adsorption, silica, alginate

Introduction

One of the biggest global problems is chemical water pollution due to growing industrial production. Phenol-type organic pollutants are often present as contaminants in wastewater from various industrial processes, such as oil refining, production of plastics, dry distillation of coal, as well as from settlements and livestock farms. Phenols are priority substances because they are toxic even in low concentrations, causing numerous harmful effects on living organisms. The World Health Organization (WHO) prescribes a maximum limit of

*e-mail: milanik@kg.ac.rs
Tel.: +381 32 303 400
Fax: +381 32 303 401
°ORCID iD: 0000-0003-4767-4419

0.001 mg/L for the presence of phenol in wastewater [1]. As a result, it must be eliminated or reduced from water and wastewater in order to safeguard human health and waterways.

Activated carbon is one of the oldest and most widely utilized adsorbents for the removal of pollutants from water. Activated carbon is typically derived from organic materials (such as coal, peat, etc.) through a costly process involving carbonization, activation, and regeneration. One of the limitations of using activated carbon is the increased carbon footprint and the consumption of a large amount of energy during production. According to some studies, obtaining activated carbon from biological materials presents a potential way to reduce the carbon footprint and energy consumption [2].

Some studies examined the removal of pollutants from water systems by activated carbon obtained from yeast biomass biochar [3-5]. Investigations into the application of composites based on activated carbon and magnetic particles are also ongoing owing to the possibility of more efficient separation from the effluent [3, 6, 7]. On the other hand, composites based on porous carbonaceous materials and magnetic particles may be unstable due to a potential leakage of Fe and Co from them, which affects the quality of treated water [8].

The immobilization of activated carbon by using adequate carriers can solve some of the above-mentioned problems [9], thus enabling its potential application in real continuous systems. The immobilization of microbial cells in alginate provides a number of advantages, such as the possibility of using a larger amount of biomass; simplicity of use; non-toxicity to humans and the environment; legal permissibility for human use; biodegradability; availability in large quantities at low cost; and the ability to easily form a gel [10, 11]. The disadvantage of using alginate in the system as a carrier is its instability in an aqueous solution for an extended period of time [11, 12].

Alginate-based composites that combine alginate with other polymers, natural and synthesized nanoparticles, microorganisms, etc., that can be used to remove pollutants from water have been extensively studied over the last decade [11, 13, 14]. Composites based on alginate and synthesized silica nanoparticles lead to an increase in mechanical strength, thermal stability, and a decrease in swelling when compared with pure alginate gels [13]. Furthermore, the obtained composites have unique physical and chemical properties, as well as compatibility when it comes to the removal of certain pollutants from water [11]. Silica is a chemically inert inorganic material that is non-toxic, stable at high temperatures, has a large specific surface area, is mechanically stable, and is resistant to the action of microorganisms and organic solvents [15, 16]. Also, the application of sol-gel technology makes it possible to obtain silica structures of different composition, morphology, and porosity in an easy and fast way [17, 18].

Some studies showed that the removal capacity of phenol from water using an alginate-activated carbon composite ranged from 1.375 mg/g [19] to 78 mg/g [20] or a silica-alginate-based composite with a removal capacity of 100.55 mg/g [21]. In some studies, the obtained removal capacity of phenol from water by hybrid systems was over 400 mg/g [22]. A few studies investigated the removal of phenol using a composite based on silica-alginate and viable microbial biomass as a result of the biological degradation of phenol by microbial enzymes. In this case, the removal efficacy ranged from 48% to 76% [23] or exceeded 90% [24]. On the other hand, there are no studies that have investigated silica-alginate-activated carbon-based composites for phenol adsorption from water.

The negative aspect of the adsorption process is the leaching of organic and inorganic matter from the adsorbent into water, which is undesirable in treated water [25]. A few studies investigated secondary contamination of treated water by applied adsorbents [25-27], and further research is needed in this regard.

Therefore, this study aimed to investigate both the adsorption properties of activated carbon obtained from pyrolysis of *S. cerevisiae* biomass and the best method for immobilization of activated carbon, in order to obtain composites with significant efficiency of phenol removal from aqueous solution and minimal leakage of organic matter from the adsorbent during the adsorption process. For this purpose, a composite based on silica, alginate, and the obtained activated carbon was used for the first time for the adsorption of phenol from water. Furthermore, the influence of contact time and the number of cycles, the leaching of organic matter from adsorbents, and adsorption kinetics experiments were studied in order to optimize the adsorption process and better understand the adsorption mechanism.

Materials and Methods

Production of *S. cerevisiae* Biomass

The strain of *Saccharomyces cerevisiae* (ATCC 2601) was maintained by subculturing on a Sabouraud Dextrose agar (SDA) (Merck) at 4ºC. The biomass of *S. cerevisiae* (ATCC 2601) was obtained by inoculation of SDA plates and incubation at 25ºC for 48 h. The culture suspension was prepared by carefully scraping the biomass with a sterile swab into sterile distilled water and then centrifuging it at 5000 rpm for 10 min (centrifuge MPV, Poland). The yeast biomass was dried at 25ºC for 12 h and ground into fine particles.

Activation and Pyrolysis of *S. cerevisiae* Biomass

The activation and pyrolysis of *S. cerevisiae* microbial biomass were performed according to a modified method carried out by Wu et al. [28]. The biomass of *S. cerevisiae* cells was used to obtain

activated carbon (Sc sample). The activation procedure was carried out by mixing 7.6 g of wet (twice washed with distilled water) biomass of *S. cerevisiae* with 12.9 g of K_2CO_3 and then by drying the obtained mixture at 100ºC.

After impregnation and drying, the yeast samples were placed in a tubular furnace (Carbolite) in an inert nitrogen atmosphere at 500, 600, 700, and 800ºC, and the obtained samples were marked as Au-500, Au-600, Au-700, and Au-800, respectively. After being cooled to room temperature, the samples were ground to a fine powder and then washed with 10% (w/v %) HCl and then with distilled water. The samples were then dried at 100ºC (12 h) and stored until use.

Immobilization of Activated Carbon Obtained from *S. cerevisiae* Biomass

The immobilization of selected activated carbon obtained from pyrolysis of *S. cerevisiae* biomass (Au-600 sample) was carried out using silica, alginate, and silica-alginate, respectively, according to the method performed by Stanojević-Nikolić et al. [29], with the condition that the immobilization of activated carbon Au-600 in silica-alginate was carried out in a ratio of alginate to silica 1:1 (AS1-P composite) and 2:1 (AS2-P composite). Briefly, silicate solution ($n(Na_2O)/n(SiO_2)$ = 0,4; $c(SiO_2)$ = 75.4 g/L) was previously passed through a cation exchange resin (Amberlite IRC1 H, Supelco). Afterwards, 0.325 g of activated carbon (Au-600) or native biomass of *S. cerevisiae* was mixed with silicate solution and 5% w/v sodium alginate solution. The mixture was added to previously prepared 55 mL of 0.1 M calcium chloride solution to form beads. The beads were then washed, dried at room temperature, and stored until use. The same procedure was applied in the case of immobilization of activated carbon (Au-600) in alginate (sample A-P), except for the addition of silicate solution.

The immobilization of selected activated carbon (sample Au-600) and native biomass of *S. cerevisiae* using silica was performed in the following procedure: 0.546 g of activated carbon/ native biomass of *S. cerevisiae* were dispersed in 15 mL of silicate solution ($n(Na_2O)/n(Si0_2)$ = 0,4; $c(Si0_2)$ = 75.4 g/L). The sulfuric acid (1 mol/L) was added into the stirred dispersion at 40ºC, allowing the entrapment of activated carbon/native biomass of *S. cerevisiae* within the formed silica gel. The obtained composites (samples S-P and S-Sc) were washed with distilled water (three times), dried at room temperature, and then crushed into fine powder particles.

The preparation of alginate beads (sample A) was carried out by dissolving 0.5 g of sodium alginate in 10 mL of distilled water, and then the mixture was added to a previously prepared 55 mL of 0.1 M calcium chloride solution. The obtained beads were subsequently rinsed three times in distilled water and ambient-dried.

Silica (sample S) was obtained by slowly adding sulfuric acid (1 mol/L) dropwise to 15 mL of sodium silicate solution ($n(Na_2O)/n(Si0_2)$ = 0,4; $c(Si0_2)$ = 75.4 g/L) at a temperature of 40ºC, which induced the synthesis of silica nanoparticles and formation of silica gel. The obtained material was washed three times with distilled water, dried at room temperature, and then crushed into fine powder particles.

Batch Adsorption Experiments

The batch adsorption process with Au-500, Au-600, Au-700, and Au-800 adsorbents was performed by weighing 50 mg of adsorbent and placing it in a cuvette containing 10 mL of initial phenol solution (100 mg/L) at pH 6 and ambient temperature under magnetic stirring (150 rpm) for 60 min. The aliquots of samples (100 µL) were taken at certain time intervals in order to determine the required contact time for phenol adsorption. The adsorbents and adsorbate were separated by centrifugation (5000 rpm for 5 min) (centrifuge MPV, Poland). The aliquots of the resulting supernatants (40 µL) were added to headspace vials with the addition of an internal standard (benzaldehyde) at a concentration of 1 mg/L.

The efficiency of phenol removal from the water model using alginate, silica, and composites was determined by dispersing 0.2 g (samples A, A-P, AS2-SC, AS1-P, and AS2-P) or 50 mg (samples S, S-Sc, and S-P) of the materials in an aqueous solution of phenol with an initial concentration of 30 mg/L, at pH 6 and ambient temperature. The saturation time of the adsorbent was determined as previously mentioned in the part of the determination of the required contact time for phenol adsorption.

A solid-phase microextraction fiber (SPME Fiber C-WR-95/PDMS, Agilent Technologies) was used for the extraction of phenol. Phenol detection was performed using a mass spectrometer (Agilent Technologies 5977AMSD) coupled to a GC unit using SIM mode.

Phenol removal was calculated as follows (Eq. (1)) [30]:

$$q_e = \frac{(C_o - C_e)}{m} \cdot V \tag{1}$$

where q_e is the amount of adsorbed phenol per unit mass of the tested adsorbent (mg/g); C_o and C_e are the initial and equilibrium concentration of phenol (mg/L), respectively; V is the solution volume (L), and m is the mass of the adsorbent (g).

Removal efficiency η_a (%) of the adsorbent was calculated as follows (Eq. (2)) [30]:

$$\eta_a = \frac{C_o - C_e}{C_o} \tag{2}$$

The Influence of Contact Time and Number of Cycles on Phenol Adsorption

The effect of contact time on phenol adsorption was determined in a batch process by using A-P, AS1-P, and AS2-P composites at ambient temperature and pH 6, at different time intervals.

Repeated consecutive cycles of phenol adsorption using A-P, AS1-P, and AS2-P composites were performed according to the above-described batch adsorption procedure, provided that in each subsequent adsorption cycle, a new quantity of phenol solution (10 mL) of initial concentration of 30 mg/L and adsorbent that was already used in the previous cycle were added to the cuvette.

Testing the Leaching of Organic Matter from Adsorbents

The leaching of organic matter from A-P, AS1-P, and AS2-P composites (0.2 g per sample) was examined during 5 cycles of incubation in distilled water (for 1200 min per cycle). In each subsequent leaching cycle, a new quantity of distilled water (10 mL) and the adsorbent already used in the previous cycle were added to the cuvette. After each agitation cycle, the supernatant was collected, and a leaching test was conducted by means of a digestion unit (AL 125) and a photometer (Photometer System AL200) (Tintometer GmbH, Dortmund, Germany). The organic matter content is expressed as chemical oxygen demand (COD) (mgO_2/L). The leaching experiments were performed in three replicates, and mean values were used in the analysis of the results. MS Excel (Microsoft Corporation, Redmond, WA) was used to calculate the mean and standard deviation.

Characterization of Adsorbents

The Scanning Electron Microscope (SEM) JSM-6390 LV JEOL, operating at 30 kV, was used to observe the morphology of samples. Before the SEM analysis, the samples were sputtered with gold. The distribution of the elements in the composites was determined with the EDS detector (Oxford Instruments X-MaxN) coupled to the SEM system.

The specific surface area and porosity of the adsorbents were measured by the method of low-temperature physical adsorption of N_2 and the BET adsorption isotherm equation. The pore volume was determined by using the Barrett-Joyner-Halenda (BJH) model. Prior to the analysis, the samples selected for determining the specific surface area and porosity of the adsorbents were thermally treated at 500ºC (due to the elimination of organic matter).

The zeta potential (ζ- potential) of silica particles was measured by dynamic light scattering (Zetasizer Nano ZS, Malvern Instruments).

IR spectra were recorded on a Thermo Scientific Nicolet Sumit FT-IR spectrometer, using the attenuated total reflectance (ATR) technique with a diamond crystal (Smart Orbit, Thermo Scientific, Madison, WI, USA). Spectral data were collected in the mid-IR range (4000-400 cm^{-1}) with 32 scans and 4 cm^{-1} resolution. Before recording each sample′s spectrum, the background spectrum (16 scans) was recorded before every sample spectrum.

Adsorption Kinetic Experiments

All the kinetics tests were performed in a series of 50 mL cuvettes containing phenol solutions (at a concentration of 30 mg/L and composite dose of 5 g/L) at pH 6 and room temperature, under magnetic stirring (150 rpm). At different time intervals of 150, 300, 400, 600, and 1200 min, the samples were collected for analysis. The repeated-cycle kinetics tests (A-P and AS2-P samples) were performed according to the described procedure, provided that a new quantity of phenol solution at the initial concentration of 30 mg/L was added in each subsequent adsorption cycle to the adsorbent already used in the previous cycle.

Phenol removal by samples at a specific time was calculated as follows (Eq. (3)) [30]:

$$q_t = \frac{(C_o - C_t)}{m} \cdot V \tag{3}$$

where q_t is the amount of adsorbed phenol at time t (mg/g); C_o and C_t are the initial and remaining concentrations of phenol in solutions before reaction and at time t (mg/L), respectively; V is the solution volume (L), and m is the mass of the adsorbent (g).

Four models (linear forms), the pseudo-first-order kinetic model, the pseudo-second-order kinetic model, the intraparticle diffusion model, and the Boyd model were used to investigate the mechanism of phenol adsorption on composites (A-P, AS2-P, and AS1-P).

The first-order kinetic model can be expressed by the following equation (Eq. (4)) [31]:

$$\ln(q_e - q_t) = -k_1 t + \ln q_e \tag{4}$$

where q_e and q_t are the amount of phenol adsorbed (mg/g) at equilibrium and at time t (min), respectively, and k_1 (min $^{-1}$) is the first-order adsorption rate constant. The values of the adsorption rate constant at room temperature were calculated from the plots of ln (q_e - q_t) versus t.

The pseudo-second-order mechanism can be expressed by the following equation (Eq. (5)) [31]:

$$\frac{t}{q_t} = \left(\frac{1}{q_e}\right) t + \frac{1}{k_2 q_e^2} \tag{5}$$

where k_2 (g/mg min) is the rate constant of the second-order adsorption, and $h = k_2 q_e^2$ is the initial adsorption rate [31]. The values of the adsorption rate constant at

room temperature were calculated from the linear plots of t/q_t vs t.

The intraparticle diffusion model was used to describe the diffusion mechanism using the following equation (Eq. (6)) [32]:

$$q_t = k_p t^{1/2} + L \tag{6}$$

where q_t is the amount of phenol adsorbed (mg/g) at equilibrium at time t (min), L is the intercept on the y/ axis and k_p (mg/g·min$^{-0,5}$) is the intraparticle diffusion rate constant, both calculated from the plot of q_t vs $t^{1/2}$. If the plot of q_t vs $t^{1/2}$ is a straight line and passes through (0,0), the intraparticle diffusion is the controlling process. In other cases, adsorption is controlled by multiple processes [33].

The Boyd model can be expressed by the following equation (Eq. (7)) [34]:

$$F = \frac{q_t}{q_e} = 1 - \frac{6}{\pi^2}\sum_{n=1}^{\infty}\frac{exp^{-n^2 B_t}}{n^2} \tag{7}$$

where F is the ratio of adsorbate adsorbed at time t (q_t) and at equilibrium (q_e).

The limiting step of adsorption based on this model can be defined by determining the value of B_t for each F from the Reichenberg table [35]. If the plot of B_t vs t is a straight line and passes through (0,0), the adsorption process is controlled by intraparticle diffusion.

Results and Discussion

Selection of the Best Activated Carbon Obtained by Pyrolysis of *S. cerevisiae* Biomass

Fig. 1 shows the results for the efficiency of phenol removal from aqueous solution at the initial concentration of 100 mg/L using viable cells of *S. cerevisiae* (sample Sc) and activated carbons (Au-500, Au-600, Au-700, and Au-800 samples).

The efficiency of phenol removal from aqueous solution was higher with activated carbons obtained from yeast biomass *S. cerevisiae* when compared to native cells of *S. cerevisiae*. The phenol removal efficiency increased with the rise of activation temperature of the obtained activated carbons and ranged from 92.4% (Au-500) to 97.1% (Au-800). The activated carbons obtained at 600 and 700°C showed similar phenol removal efficiency (96.55% and 96.87%), while the activated carbon obtained at a temperature of 500°C showed lower removal efficiency. Similar results were obtained by some studies [4, 36].

In this study, the activated carbons obtained from *S. cerevisiae* yeast biomass in the temperature range of 600-800ºC had very similar adsorption capacities for phenol removal. Therefore, the immobilization studies were conducted using activated carbon obtained at an activation temperature of 600°C.

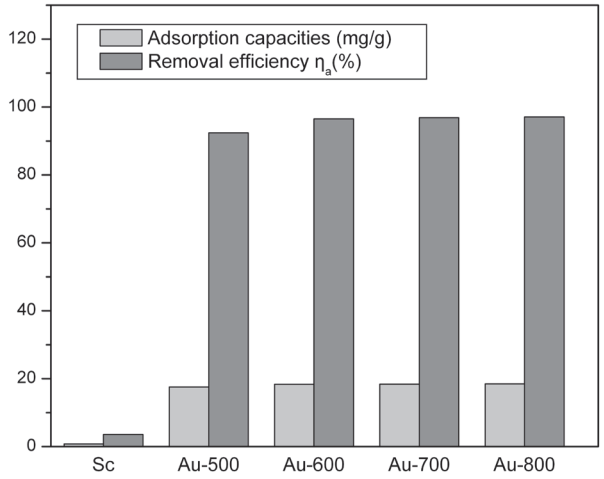

Fig. 1. The efficiency of phenol removal from aqueous solution using viable cells of *S. cerevisiae* (sample Sc) and activated carbons: Au-500, Au-600, Au-700, and Au-800.

Morphology of Adsorbents

The SEM micrograph of activated carbon obtained by pyrolysis of yeast biomass *S. cerevisiae* at 600ºC (sample Au-600) is shown in Fig. 2. The aggregates had dimensions of 4 to 22 μm, while the dimensions of the cavities ranged from 0.4 to 1.2 μm and represented the dimensions of yeast cells (Fig. 2b)).

Fig. 3 shows the SEM micrographs of the external (Figs 3a) and 3b)) and the internal (Fig. 3(c-f)) morphology of A-P composite obtained in cross-section. The external surface is rough, and fragments of pyrolyzed yeast are distributed in the alginate matrix (Fig. 3b)). Fig. 3(c-f) shows fragments of pyrolyzed yeast in the alginate cavities. The cavities are ellipsoidal in shape, with dimensions between 30 and 80 μm, filled with pyrolyzed yeast (Figs 3c) and d)). Figs 3e) and 3f) show the morphology of pyrolyzed yeast immobilized in the alginate matrix.

Fig. 4 and Fig. 5 show the SEM micrographs of the morphology of silica-alginate-activated carbon composites (AS2-P and AS1-P samples) obtained at different mass ratios of alginate to silica (2:1 and 1:1) during the synthesis, respectively. Fig. 4a) and 4b) show the external morphology of AS2-P composite, while Figs 4c) and 4d) show the external morphology of AS1-P composite. The obtained composites are ellipsoidal, with a diameter of approximately 1.5 mm. The external surface is rough and exhibits silica and pyrolyzed yeast particles dispersed throughout the alginate matrix. A significant proportion of ellipsoidal particles, with dimensions of about 1 μm, represents deposited silica particles on the surface of AS1-P composite (Fig. 4d)).

Fig. 5 shows the internal morphology of AS2-P (Fig. 5(a-d) and AS1-P (Figs 5e) and 5f)) composites.

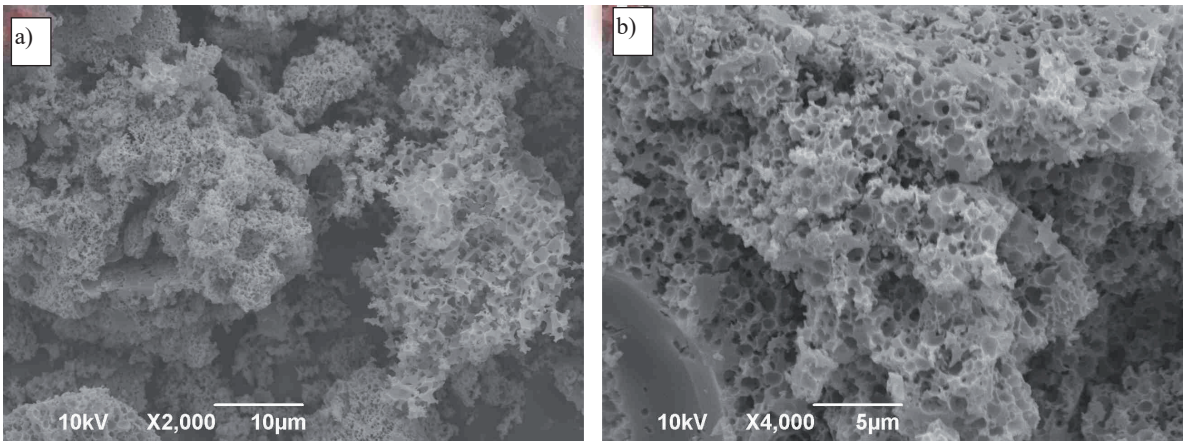

Fig. 2. SEM micrograph of activated carbon (sample Au-600) at different magnifications. a) 2000× and b) 4000×.

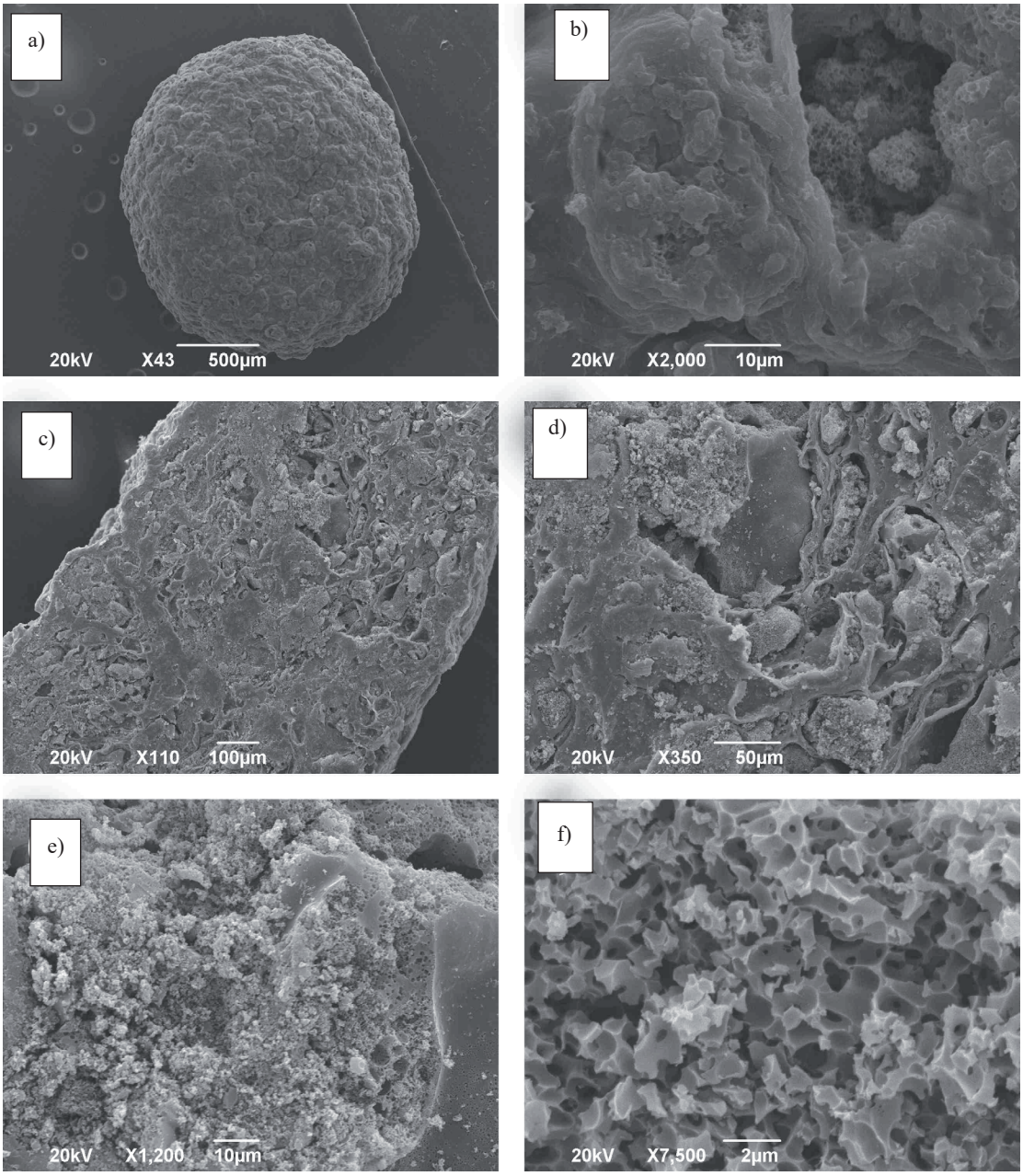

Fig. 3. SEM micrographs of the A-P composite. (a, b) outer surface and (c, d, e, f) cross-section.

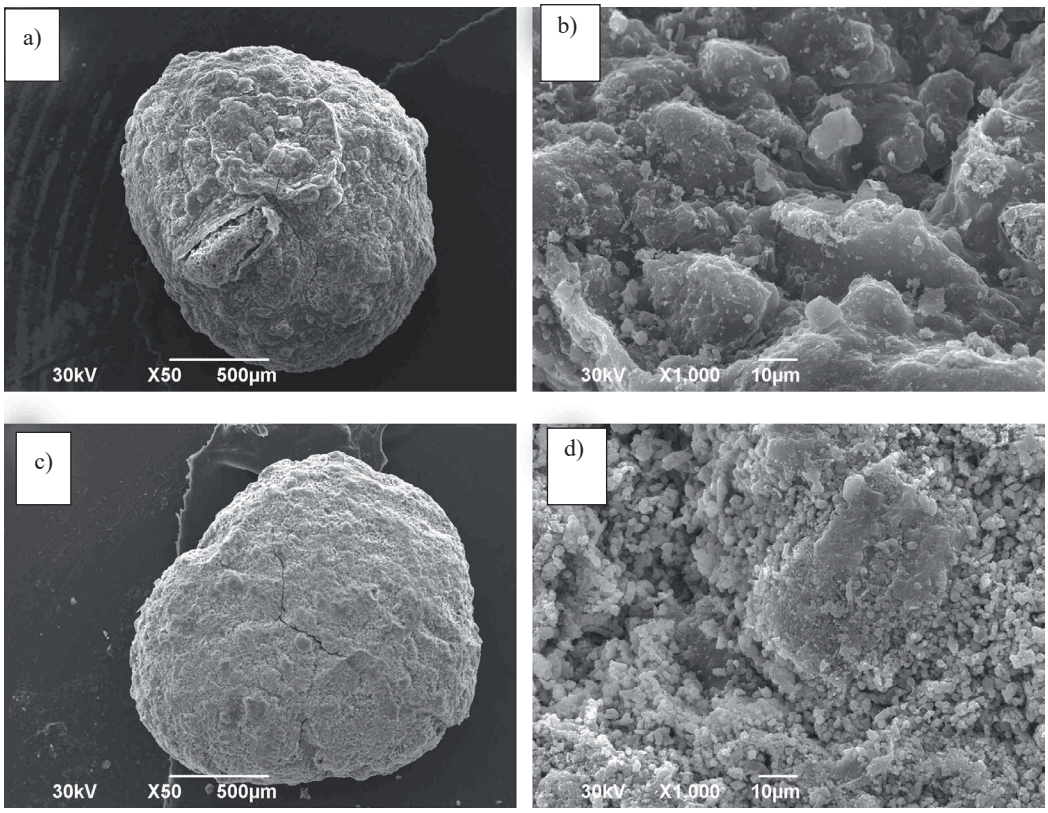

Fig. 4. SEM micrographs of the surface of silica-alginate-activated carbon composites. (a, b) AS2-P and (c, d) AS1-P.

Figs 5b) and 5c) show macrovoids with dimensions of about 10 µm. The macrovoids originate from the alginate hydrogel that forms a highly porous structural network [37]. Fragments of pyrolyzed yeast are also observed in the internal morphology of AS2-P composite (Fig. 5d)). In Figs 5e) and 5f), the internal morphology of AS1-P composite is shown, where a significant proportion of mesoporous silica is observed.

Figs 6a) and 6b) show the EDS mapping of elements in AS2-P and AS1-P samples, respectively. Fig. 6a) shows voids with dimensions of around 10 µm (AS2-P sample), while Fig. 6b) shows smaller voids in the range of 0.5 to 4 µm (AS1-P sample), with a higher proportion of smaller voids. This indicates the influence of silica concentration on the dimensions of alginate voids, where the increasing silica concentration (AS1-P sample) reduces the dimensions of the voids, which may potentially affect the diffusion of pollutants within the composite.

The EDS mapping of individual elements shows a more uniform distribution of elements in the AS1-P (Fig. 6d)), probably due to the smaller dimensions of the voids. The dark regions in AS2-P samples represent larger voids (Fig. 6c)). As expected, the presence of Si and O atoms is more pronounced in the AS1-P sample than in the AS2-P sample.

Porosity and BET Surface Area Measurement of Adsorbents

The results of low-temperature physical adsorption of N_2 for AS2-P and AS1-P composites are shown in Fig. 7a). In order to remove the organic part of the composite, the samples were annealed at 500ºC, therefore the results primarily relate to the properties of silica and activated carbon that constitute the tested composites.

The textural properties of the samples, derived from the nitrogen isotherms, reveal that the majority of the total BET surface of the samples can be ascribed to their external surface. The t-plot of AS1-P (not presented here) indicates the presence of a small amount of micropores, while for AS2-P, the t-plot is typical for non-porous materials. However, the external surfaces of both samples show the presence of mesopores/surface roughness (Table 1, Fig. 7b)). Possibly, macropores are also present, judging by the significant increase in nitrogen adsorption at high relative pressures. The BET surface of AS1-P was found to be twice as large as that of AS2-P. In the case of AS1-P, some 20% of the BET surface can be attributed to micropores (Table 1).

Fig. 7b) shows the pore size distribution of the samples of AS2-P and AS1-P composites. The pore size distribution in the silica of the AS2-P sample is wider with a higher proportion of larger pores. Small peaks are present at around 6 nm, which probably represent the pore sizes in activated carbon. On the other hand, the pore size distribution in the AS1-P sample is narrower,

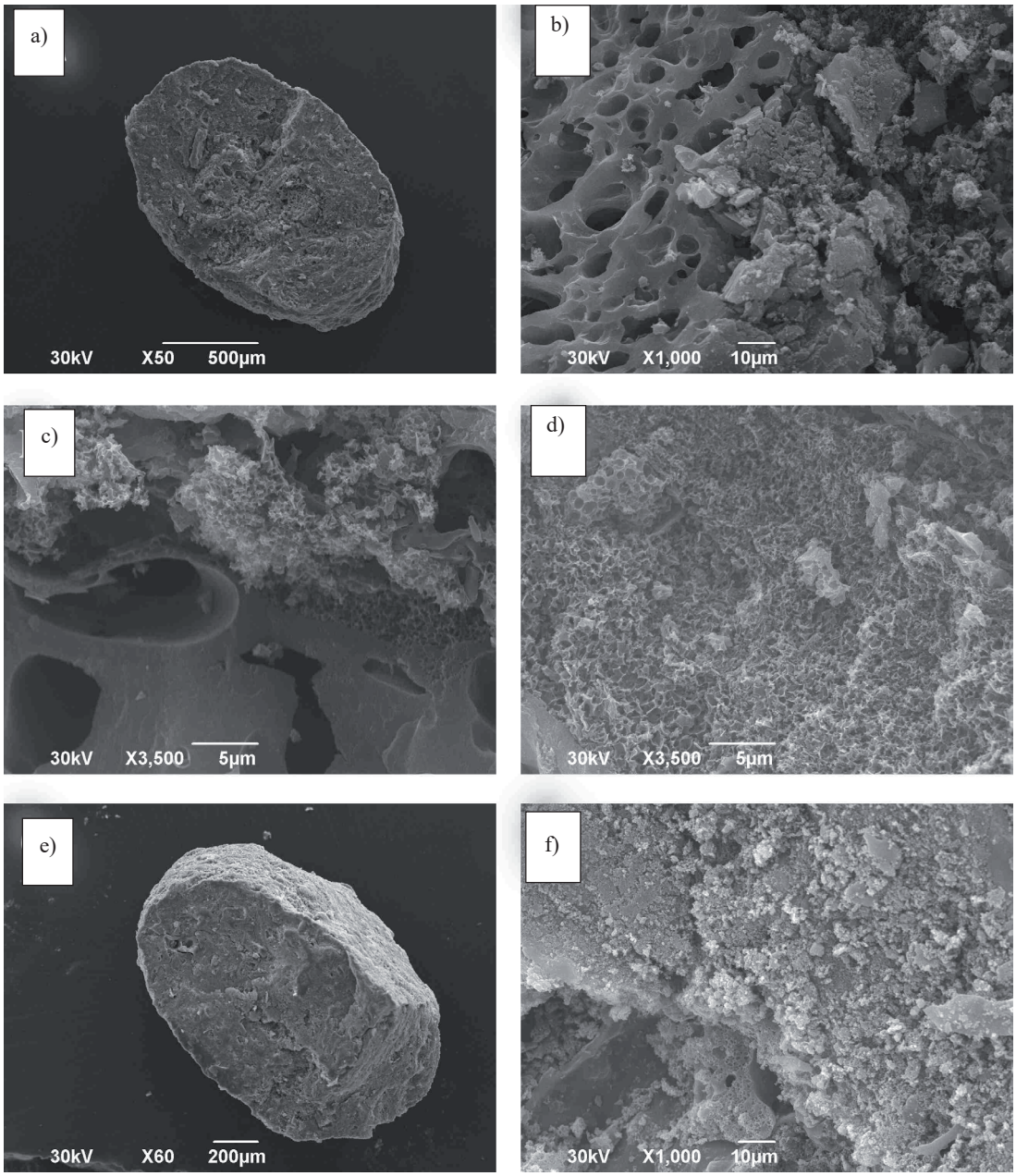

Fig. 5. SEM micrographs of the cross-sectional area of the internal morphology of (a, b, c, d) the AS2-P and (e, f) AS1-P composites.

and compared to the AS2-P sample, it is shifted towards somewhat smaller mesopores.

Table 1 shows the results of total surface area (S_{BET}), external surface area (S_{ext}), total pore volume (V_{tot}), micropore volume (V_{micro}), and average pore diameter of AS2-P and AS1-P composites.

The AS1-P sample had a slightly larger surface area and pore volume. As shown in Table 1, the total surface area mainly derives from the external surface of silica, which was evident in the AS2-P sample. The average pore diameter is larger in the AS2-P sample and is 31.7 nm, while in the AS1-P sample, it is 15.2 nm. Both samples are characterized by negligible microporosity and are mainly dominated by mesopores.

FT-IR Spectrum Analysis

The FT-IR spectrum of activated carbon (Fig. 8a)) prepared from *S. cerevisiae* biomass was determined to characterize the nature of the functional groups present on the surface of the activated carbon. There are overlapping vibrations in the range of 3800-1800 cm^{-1}. The sharp peak at 3727 cm^{-1} is assigned to stretching vibrations of free O–H groups without hydrogen bonds [38]. On the other hand, a broad peak, typically between 3600 and 3100 cm^{-1}, can be assigned to intermolecularly hydrogen-bonded hydroxyl (O–H) groups [39]. The band around 1615 cm^{-1} is assigned to aromatic C=C stretching, indicating the formation of aromatic ring structures during carbonization. The band at 1266 cm^{-1} may be due to the existence of C–O–C,

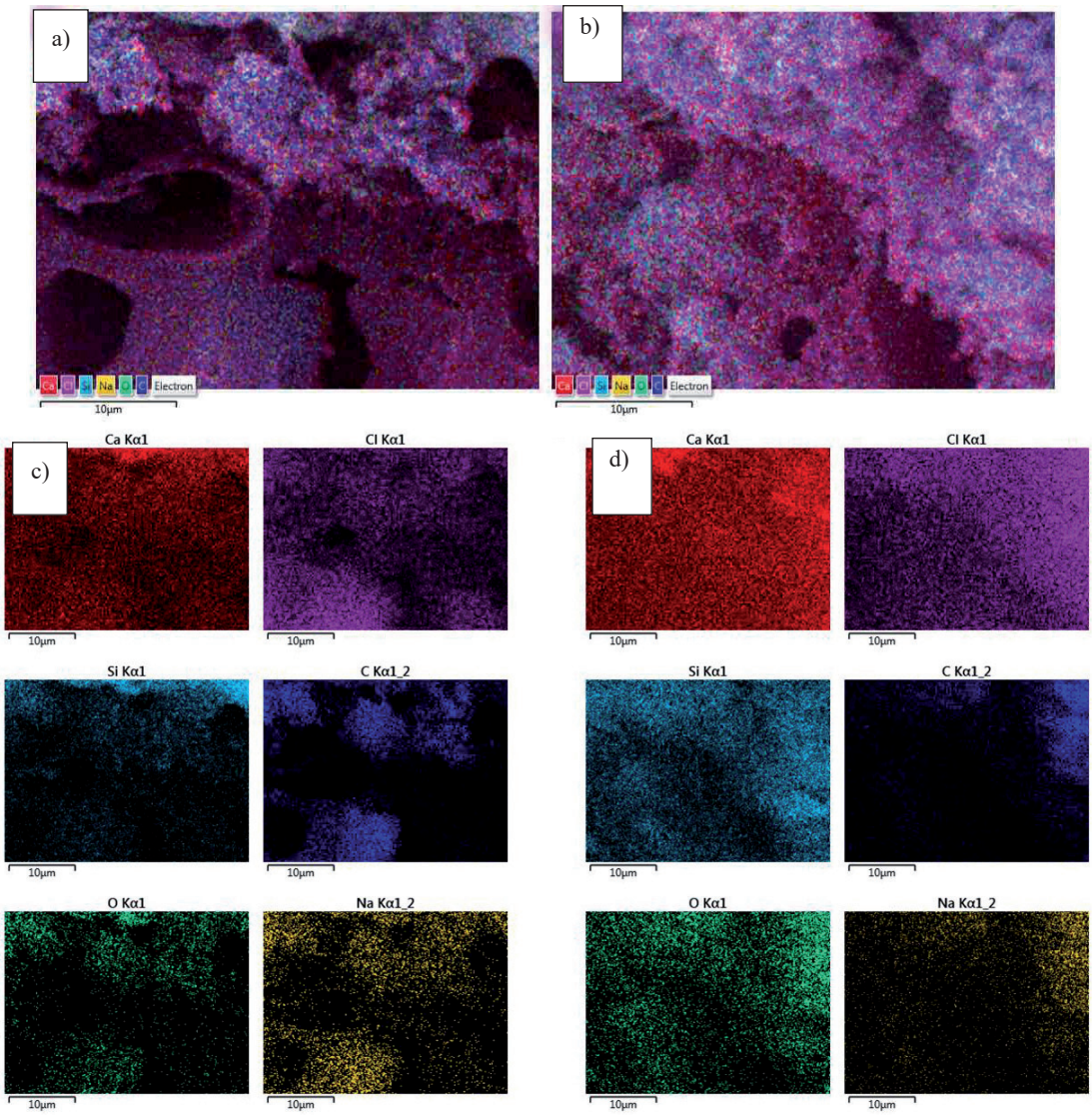

Fig. 6. EDS mapping of the cross-sectional area of a) AS2-P and b) AS1-P composites and (c, d) elements, respectively.

C–O, and O–H bonds, i.e., alcoholic and carboxylic groups [40].

The FT-IR spectrum of alginate-activated carbon yeast biomass is shown in Fig. 8b). The peaks at 1592.4 and 1414.8 cm^{-1} are assigned to asymmetric and symmetric COO– (carboxylate) stretching vibration, respectively [41]. The band at 1295 cm^{-1} was attributed to the C–O stretching vibration. The peak at around 1081 cm^{-1} is related to C–O, C–C, and COC stretching vibrations. The peak at 1028 cm^{-1} is also assigned to C–C and COC vibrations in alginate [41].

The FTIR spectrum of pure silica powder obtained by acidic neutralization of highly basic sodium silicate solution is shown on Fig. 8c). The bands at ~462.69, 798.6 and 1081.8 cm^{-1}, which appear in the spectrum of silica, can be attributed to bending, symmetric stretching and asymmetric stretching vibration or bending vibration of Si-O-Si bonds, respectively [42].

Fig. 8d) shows the FT-IR spectrum of the alginate-silica-activated carbon composite (sample AS2-P). The spectrum revealed the shift of the absorption band observed in pure silica at 1081.8 cm^{-1} to a lower frequency at 1057.7 cm^{-1}. This can be explained by

Table 1. Porosity and surface characteristics of AS2-P and AS1-P composites.

Samples	S_{BET} (m^2/g)	S_{ext} (m^2/g)	V_{micro} (cm^3/g)	V_{tot} (cm^3/g) at p/p_0=0,99	Average pore diameter (nm)
AS1-P	59	48	0.004	0.28	15.2
AS2-P	27	26	0.0002	0.21	31.7

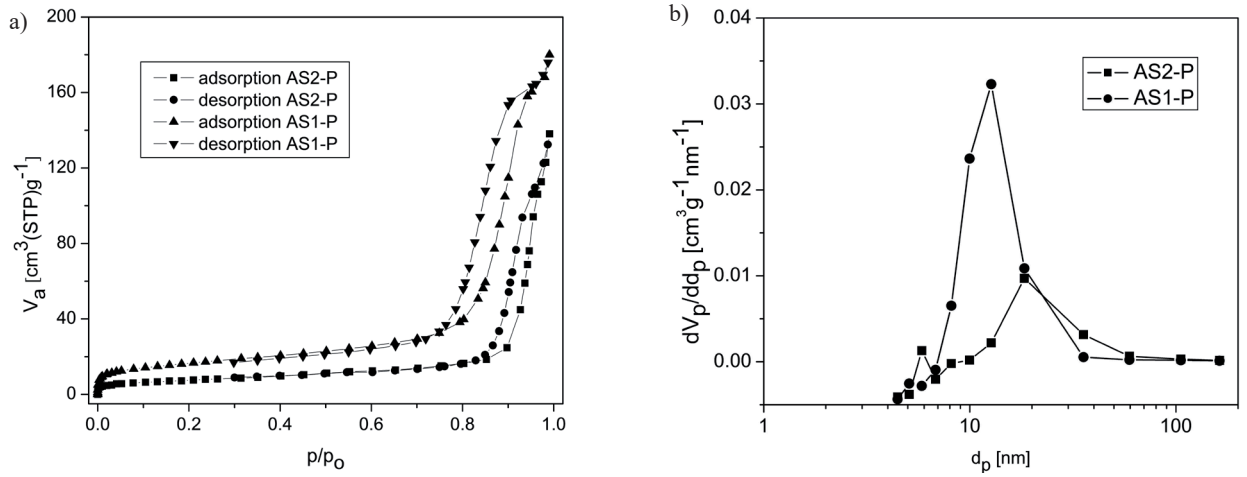

Fig. 7. a) Adsorption and desorption isotherms and b) pore size distribution of AS2-P and AS1-P composites.

the formation of a strong interaction between silica nanoparticles and calcium alginate matrix, resulting in weakening of the strong Si–O bonds. Moreover, alginate-silica interactions prevented shrinkage or structural collapse of silica gel during gelation and drying, promoting the formation of a more open and porous structure induced by the polymer network [43].

It was also confirmed by EDS mapping and low-temperature nitrogen adsorption. EDS mapping showed uniformly distributed silicon and oxygen atoms inside

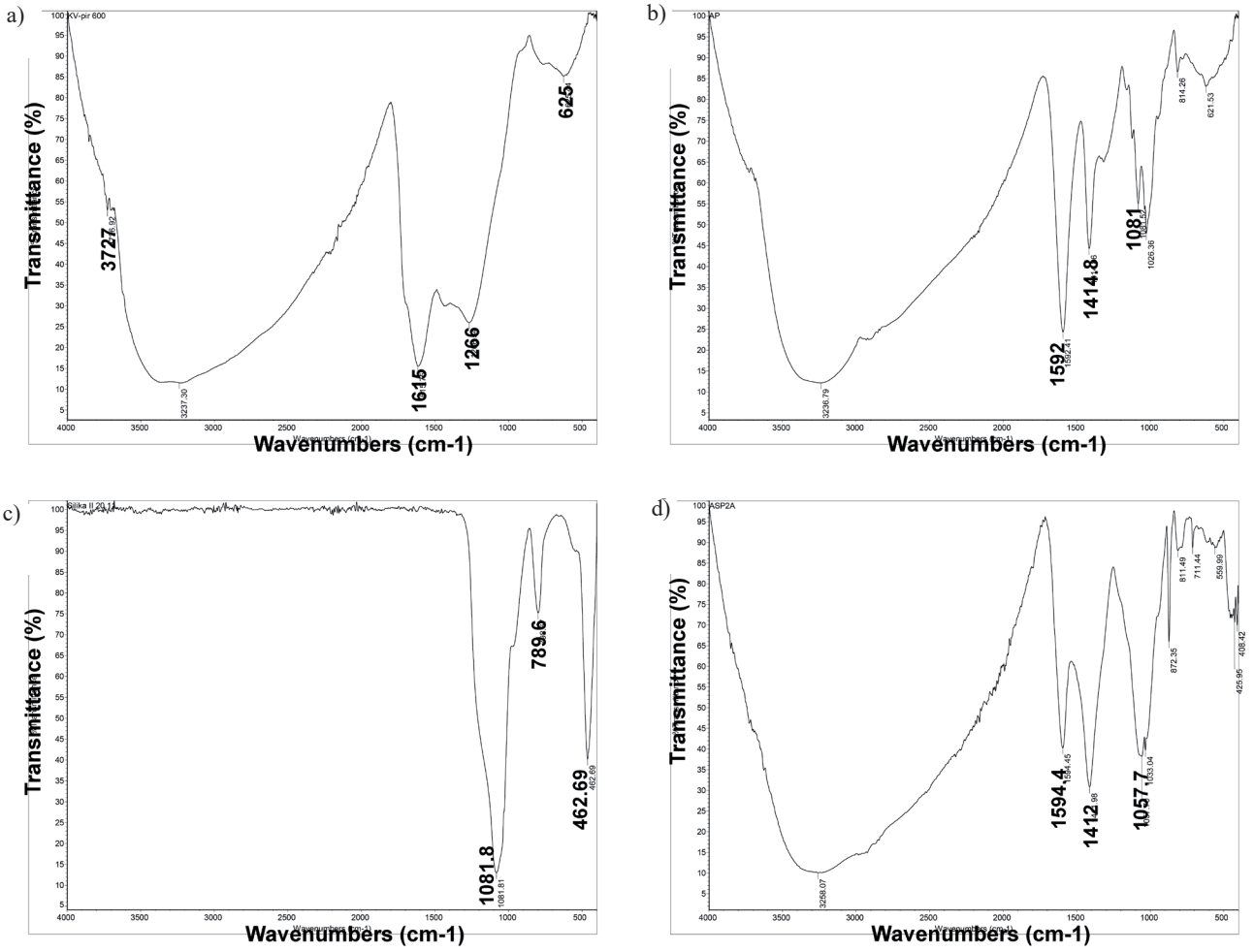

Fig. 8. FT-IR spectrum of a) activated carbon from *S. cerevisiae* biomass, b) alginate-activated carbon composite based on yeast biomass, c) silica powder, and d) alginate-silica-activated carbon composite (sample AS2-P).

the composite bead, revealing the absence of silica shrinkage. The domination of the external surface and weak porosity of silica also revealed the absence of shrinkage. The FT-IR spectrum of AS2-P composite also revealed a decrease and an increase in asymmetric and symmetric COO– stretching vibrations (peaks at 1594.4 and 1412 cm^{-1}), respectively. This can also be assigned to silica-alginate interaction.

Adsorption Experiment Results

Fig. 9 shows the results for phenol removal efficiency from water at the initial concentration of 30 mg/L, using silica (S), alginate (A), and S-Sc, S-P, A-P, AS2-Sc, AS1-P, and AS2-P composites.

Silica (sample S) has no affinity for phenol, probably due to the presence of a large number of silanol groups on the adsorbent, which make the adsorbent surface hydrophilic [44]. As shown in Fig. 10, silica is strongly

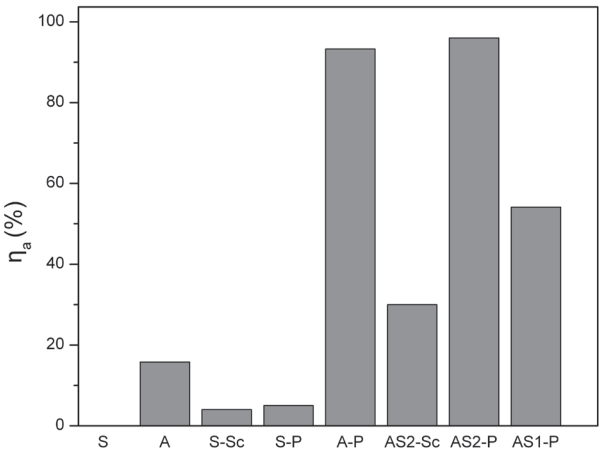

Fig. 9. Phenol removal efficiency from a water model using silica, alginate, and activated carbon-based composites (S-Sc, S-P, A-P, AS2-Sc, AS1-P, and AS2-P).

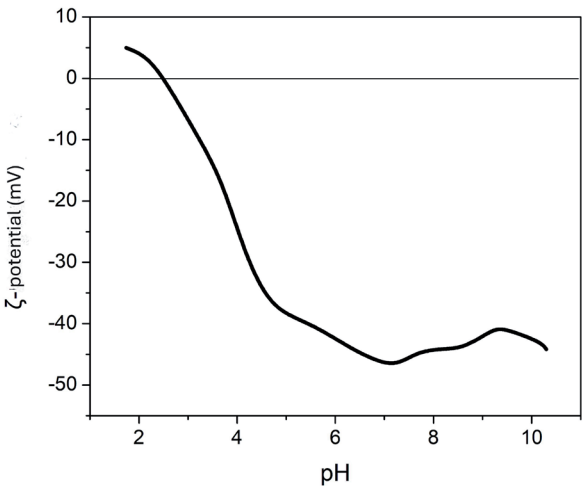

Fig. 10. Dependence of ζ-potential on pH for silica (sample S).

negatively charged at the tested pH and can also repel negatively charged dissociated phenol molecules.

The S-Sc and S-P composites showed low phenol adsorption efficiency (Fig. 9). The composite of silica and activated carbon (S-P) showed a slightly higher efficiency (5%) compared to the S-Sc sample, which amounted to 4%. The efficiency of phenol removal from water by the AS2-P composite was higher by 1, 1.7, 3.2, 19.2, and 24 times than that of the A-P, AS1-P, AS2-Sc, S-P, and S-Sc composites, respectively.

The significant influence of the structure and composition of the obtained composites on phenol removal efficiency is evident. Since the pore size distribution in the silica of the AS2-P sample is wider, with a higher proportion of larger pores (Fig. 8b)), a higher removal efficiency of phenol was expected compared to the AS1-P sample. The presence of silica in composites affected phenol removal efficiency, since the A-P sample has higher removal efficiency compared to some silica-containing composites (AS1-P, AS2-Sc, S-P, and S-Sc samples). Generally, the optimal composition and microstructure of composites for phenol removal were reported for the AS2-P sample, with a silica-alginate ratio of 1:2.

Some studies reported phenol removal efficacy of ≥48% by silica-alginate-fungus biocomposites [23]. Essifi et al. [45] confirmed effective removal of phenol and its chlorinated derivatives from water by alginate montmorillonite hybrid microcapsules. Shim et al. [24] reported the removal efficiencies of phenol, copper, and cadmium ions by silica-alginate-bacterial biomass composites in the simultaneous process of 93%, 98%, and 99%, respectively.

Effect of the Number of Cycles on Phenol Adsorption onto Composites

Table 2 shows the efficiencies of repeated consecutive cycles of phenol adsorption from water (at an initial concentration of 30 mg/L) carried out using A-P, AS2-P, and AS1-P composites.

The best adsorption characteristics were manifested by the AS2-P composite, whereas the weakest characteristics were manifested by the AS1-P composite. In the AS2-P composite, which also has the highest adsorption efficiency, the adsorption efficiency decreased in the fifth cycle by 12.3% compared with the first cycle. The decrease in adsorption efficiency in the fifth cycle compared to the first cycle for the A-P composite was 41.3%. On the other hand, the phenol removal efficiency of the AS1-P composite is the lowest. Based on this result, the impact of increased silica concentration on the weaker adsorption characteristics of the AS1-P composite is evident, because, as shown in Fig. 9, silica has no affinity for binding phenol. However, silica affects the structural characteristics of the AS2-P composite and the creation of a large number of small cavities, as well as the formation of narrow, tiny channels with a mesoporous structure [46] that allow

Table 2. Phenol removal efficiency using A-P, AS2-P, and AS1-P composites in five consecutive adsorption cycles.

Samples	Removal efficiency η_a (%)				
	Cycles				
	I	II	III	IV	V
A-P	93.3	86	60.9	53.57	52
AS2-P	96	93	90.1	87.2	83.7
AS1-P	54.15	47.5	45.3	42	39.5

easier and faster diffusion of phenol into the interior of the composite (Fig. 11). Moreover, the active sites in the AS2-P composite are more accessible for phenol binding, which contributes to a higher efficiency of phenol adsorption at higher cycles. However, at higher silica concentration, as was the case with the AS1-P composite, the higher proportion of silica probably closes the microcavities, thus providing more significant resistance to the diffusion of phenol into the interior of the composite.

Fig. 11 shows the schematic representation of diffusion pathways for phenol adsorption removal efficacy by silica-alginate-activated carbon composite. The external hydrodynamic layer is located around a composite bead. The composite bead is composed of both silica-alginate material and activated carbon obtained from yeast. Porous channels (shown in white) are located inside the silica-alginate material. The internal channels and cavities in the composite enable the diffusion of a pollutant towards the activated carbon located inside the composite. Diffusion resistance in mass transfer mainly occurs in porous channels.

Effect of the Contact Time on Phenol Adsorption onto Composites

Fig. 12 shows the effect of time on the efficiency of phenol adsorption by activated carbon composites (A-P, AS1-P, and AS2-P samples).

The effect of time on the process of phenol adsorption from water using the A-P composite (Au-600 in alginate) in the first, third, and fifth cycles

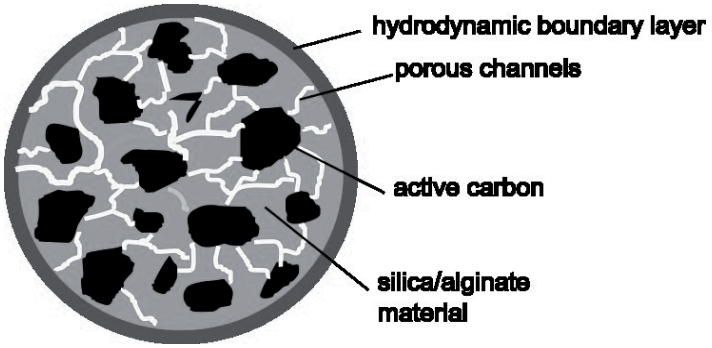

Fig. 11. Schematic representation of diffusion pathways for phenol adsorption removal efficacy by silica-alginate-activated carbon composites.

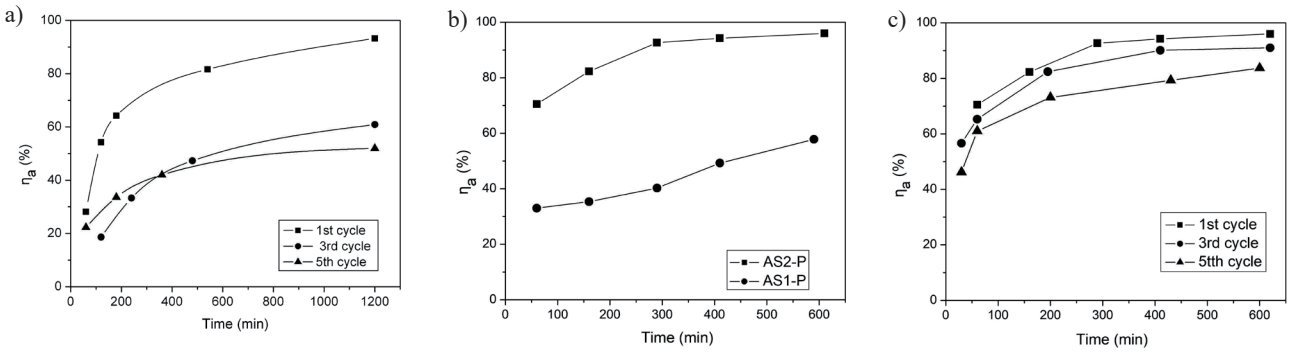

Fig. 12. Effect of time on the efficiency of phenol removal using a) the A-P composite in the first, third, and fifth cycles, b) AS1-P and AS2-P composites, and c) the AS2-P composite in the first, third, and fifth cycles.

is shown in Fig. 12a). Equilibrium was not achieved by the A-P composite even after 1200 min of contact during the first and third cycles, whereas equilibrium was achieved after 1200 min in the fifth cycle. The largest quantity of phenol binds to the outer surface of the A-P composite in the first 400 min due to the availability of a large number of active sites on the adsorbent. The subsequent adsorption process proceeds more slowly due to the reduction in the number of free active sites for binding.

The effect of time on phenol adsorption from water using the AS1-P and AS2-P composites is shown in Fig. 12b). The differences in the structure of the AS1-P and AS2-P composites (Fig. 5) affected the time required to reach equilibrium and the efficiency of phenol adsorption from water (Table 2).

Phenol adsorption using the AS2-P composite reached an equilibrium value after 410 min of contact, while adsorption using the AS1-P composite was slower and was not achieved even after 600 min (Fig. 12b)). The dimensions of a phenol molecule (0.57 nm × 0.43 nm) [30] allow its diffusion within the AS1-P and AS2-P composites. However, the surface of the AS1-P composite is dominated by silica, which has a low affinity for binding phenol. Also, the dimensions of the formed cavities and channels inside the AS1-P composite are smaller compared to those of AS2-P and provide greater resistance to mass transfer.

The effect of time on the process of phenol adsorption from water using the AS2-P composite in the first, third, and fifth cycles is shown in Fig. 12c). In the first and third adsorption cycles, equilibrium was achieved after 410 min of contact. In the fifth cycle, equilibrium was reached more slowly and was not achieved even after 600 min due to the reduction in available binding sites on the composite surface and the diffusion of phenol into the interior of the composite. On the other hand, the adsorption efficiency during the first and third cycles was similar, indicating that the AS2-P composite has significant potential for phenol removal due to its more developed porous structure (Table 1). The internal channels and cavities in the AS2-P composite enable diffusion of a pollutant towards the activated carbon located inside the composite.

Comparing the results given in Figs 12a) and 12c), it can be observed that equilibrium in all three cycles of phenol adsorption was reached faster in AS2-P compared to A-P. Also, phenol adsorption efficiency using the AS2-P composite was higher compared to A-P due to the optimal structural characteristics of the AS2-P composite, as stated above.

Leaching of Organic Matter from Composites

Table 3 shows chemical oxygen demand (COD) values after five cycles of organic matter leaching from the A-P, AS1-P, and AS2-P composites.

Table 3 shows that COD values decreased after each cycle. Compared to other composites, the leaching of organic matter was the lowest in the AS1-P composite. After the fourth and fifth cycles, the leaching of organic matter was recorded only in the A-P sample.

The leaching of organic matter from the AS1-P sample was about 1.7 times lower compared to AS2-P after the first cycle, probably due to the higher concentration of silica in the AS1-P sample. The COD values were similar after the second cycle for both samples. The presence of silica in AS1-P and AS2-P composites resulted in a decrease in the leaching of organic matter due to mechanical stability. Similar results were obtained in some studies [22].

Adsorption Kinetics

Fig. 13 shows the adsorption kinetics of phenol onto A-P, AS2-P, and AS1-P composites. Adsorption kinetics were studied at the initial phenol concentration of 30 mg/L and the adsorbent dose of 5 g/L. The saturation capacities for A-P and AS2-P samples were reached after 800 and 600 min and amounted to 1.3 and 2.3 mg/g, respectively. On the other hand, phenol adsorption onto AS1-P proceeded very slowly, and saturation was not achieved in the tested time interval.

Adsorption kinetics were considered using several linear adsorption kinetic models: the pseudo-first-order and the pseudo-second-order kinetic models, the intraparticle diffusion model, and the Boyd model.

Fig. 14 shows linear forms of the pseudo-first-order (a), pseudo-second-order (b), intraparticle diffusion (c), and Boyd (d) models for phenol adsorption onto A-P, AS2-P, and AS1-P composites. The parameters of pseudo-first-order and pseudo-second-order kinetic

Table 3. COD values for A-P, AS1-P, and AS2-P composites after five leaching cycles.

Samples	COD (mgO_2/L) (mean±SD*)				
	Cycles				
	I	II	III	IV	V
A-P	250.33±1.527	100.66±2.08	60.33±1.527	37.33±1.527	28±2.00
AS1-P	46±1.00	22.33±2.51	0	0	0
AS2-P	78.33±1.527	25.00±0.50	4.26±0.64	0	0

*standard deviation.

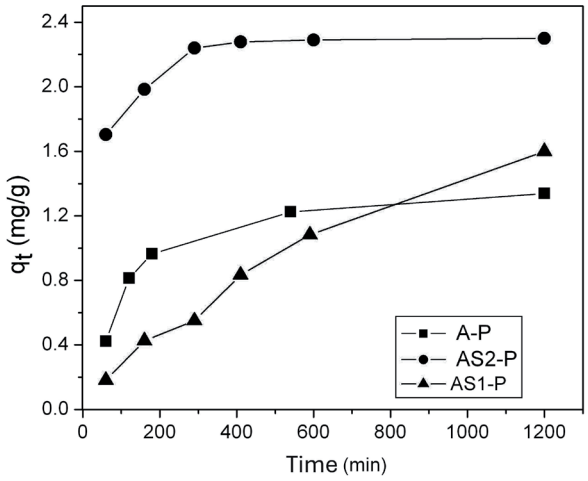

Fig. 13. Adsorption kinetics of phenol onto A-P, AS2-P, and AS1-P composites.

models for phenol adsorption onto A-P, AS2-P, and AS1-P composites are shown in Table 4.

For all samples, a better match with the experimental data was achieved with the pseudo-second-order model, as confirmed by Fig. 14b). According to the pseudo-second-order model, both adsorption and ion exchange take place on the adsorbent surface, with chemical binding to active sites as a rate-limiting step for adsorption [47].

Also, the experimentally obtained values for the adsorption capacity in equilibrium (q_e) (Fig. 13) match well the calculated values obtained pursuant to the pseudo-second-order model (Table 4).

The adsorption rate constant, k_2, and the initial rate, h, were the highest in the AS2-P sample. The structural characteristics of the composites affected the adsorption rate. AS2-P composite (Figs 5a) and 5b)) contains a large number of small cavities and narrow, tiny channels with mesoporous structure, which facilitate faster diffusion of phenol into the interior of the composite compared to A-P and AS1-P samples (Fig. 3f) and Fig. 5f)), respectively. AS1-P composite contains a higher proportion of silica (Fig. 6b)), which probably led to the closure of small cavities and higher resistance to mass transfer into the interior of the composite, and a lower rate of phenol adsorption. On the other hand, sample A-P has a lower adsorption rate compared to the AS2-P sample, but higher than AS1-P. The silica/alginate ratio in the AS2-P sample resulted in the formation of an optimal composite

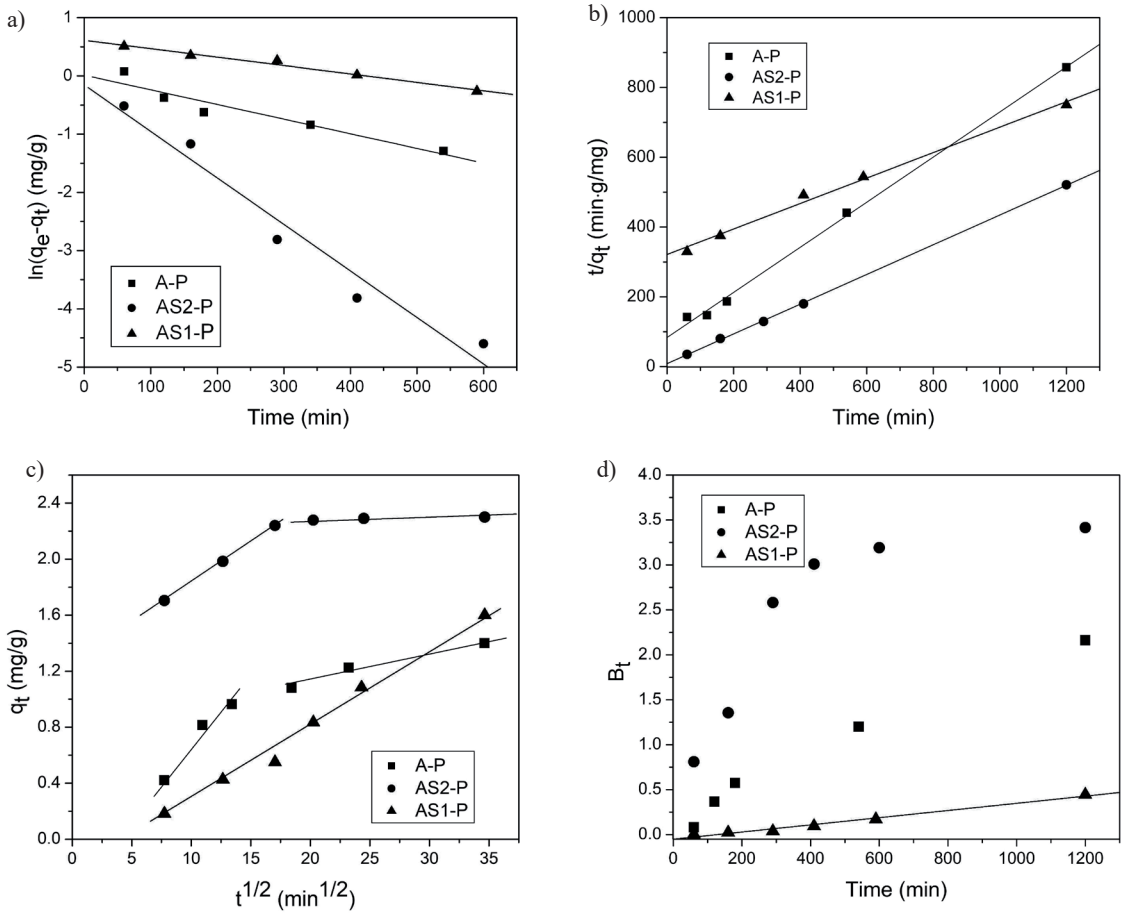

Fig. 14. Adsorption kinetic models for phenol adsorption onto A-P, AS2-P, and AS1-P composites. a) pseudo-first-order, b) pseudo-second-order, c) intraparticle diffusion, and d) Boyd models.

Table 4. Parameters of pseudo-first-order and pseudo-second-order kinetic models for phenol adsorption onto A-P, AS2-P, and AS1-P composites.

Kinetic models	Parameters	Samples		
		A-P	AS2-P	AS1-P
Pseudo-first order	q_e (mg/g)	1.01	0.86	1.85
	k_1 (mg/g·min)	0.003	0.008	0.0015
	R^2	0.914	0.961	0.983
Pseudo-second order	q_e (mg/g)	1.55	2.35	2.74
	h (mg/g·min)	0.012	0.12	0.003
	k_2 (g/min·mg)	0.01	0.02	0.0004
	R^2	0.998	0.9998	0.993

structure that allows faster and more efficient adsorption of phenol compared to the sample without added silica (A-P) or the composite with a higher quantity of silica (AS1-P).

The removal of phenol from water using activated carbon pretreated with an ionic liquid and immobilized in alginate was studied by Khan et al. [20]. In this study, it was found that the pseudo-second-order kinetic model is good for describing the adsorption process. Similar results were obtained by other authors [19, 22]. Khoy [21] proved that the adsorption process of phenol from water by silica-alginate bionanocomposite follows a pseudo-second-order kinetic model.

Using the intraparticle diffusion model, it can be determined whether the phenol adsorption process onto composites is controlled by diffusion through the outer fluid layer or by intraparticle diffusion. Fig. 14c) shows the intraparticle diffusion model for phenol removal from aqueous solution for A-P, AS2-P, and AS1-P composites.

If the graph/plot dependence of q_t on $t^{1/2}$ is multilinear, with two or more line segments, the overall rate of the adsorption process is affected by both diffusion through the outer fluid layer and intraparticle diffusion.

The graph dependence of q_t on $t^{1/2}$ for phenol removal using A-P and AS2-P composites gives a broken straight line with two segments (Fig. 14c)), which implies that intraparticle diffusion is not the only limiting step of overall adsorption. The almost horizontal position of the second segment in the AS2-P sample indicates that equilibrium is reached [48]. On the other hand, the graph dependency of q_t on $t^{1/2}$ for phenol removal using AS1-P composite shows only one linear segment that passes near the origin of coordinates. This indicates that the external diffusion dominates in the AS1-P sample, probably due to the higher concentration of silica that almost completely covers the external surface of the composite (Figs 5e) and 5f)) and thus pushes the activated carbon towards the interior of the composite. Also, compared to AS2-P, the specific surface area of silica is larger, and the pore dimensions are smaller in the AS1-P sample, which influences a greater resistance to the transfer of phenol mass to active adsorption centers.

Table 5 shows intraparticle diffusion parameters for phenol adsorption onto A-P, AS2-P, and AS1-P composites.

The value of the parameter k_p in the first segment was higher in all samples compared to the second segment. The process rate decreases in the second segment due to reduced concentration of phenol in the solution and slower diffusion of the adsorbate into the pores. The value of the parameter k_P is the highest for A-P, and the lowest for AS1-P. The higher quantity of silica in the composites (sample AS1-P) provides resistance to the transfer of phenol mass to the adsorption centers located on activated carbon. The value of the parameter L is the highest in the AS2-P sample in both segments, with the exception that, in the A-P and AS2-P samples, the value of the parameter L increases in the second segment due

Table 5. Intraparticle diffusion parameters for phenol adsorption onto A-P, AS2-P, and AS1-P composites.

Parameters	Step 1			Step 2		
	Samples			Samples		
	A-P	AS2-P	AS1-P	A-P	AS2-P	AS1-P
k_P (mg/g·min$^{1/2}$)	0.097	0.058	0.054	0.019	0.001	-
L (mg/g)	-0.276	1.257	-0.268	0.755	2.25	-
R^2	0.969	0.9999	0.9899	0.968	0.921	-

to an increase in the thickness of the outer layer and hindered external diffusion.

Based on the slopes of line segments, the rate of diffusion into the pores of the adsorbent can be determined. The slope of the first segment is the highest in the A-P composite. This indicates that the rate of phenol diffusion into the pores of A-P composite is also higher than in both AS2-P and AS1-P composites, due to the presence of silica in these two samples, which provides resistance to the transfer of phenol into the interior of the composite. The slopes of line segments in the A-P and AS2-P samples are smaller in the second segment compared to the first segment. This indicates a lower rate of phenol diffusion into the pores of adsorbents, which was also registered based on the parameter k_P.

The removal of phenol from water using activated carbon obtained from the plant *Calligonum polygonoides* immobilized in alginate was studied by Khan et al. [20]. The results of this study showed that two segments were determined for both samples using the Weber and Morris model, which means that, in addition to intraparticle diffusion, the rate of phenol removal from water is also affected by external diffusion.

The Boyd model is applied to verify if the adsorption process is controlled by external (film) diffusion or intraparticle diffusion [20]. Fig. 14d) shows the dependence of B_t vs t during the phenol adsorption with A-P, AS2-P, and AS1-P composites. As can be seen from Fig. 14d), the plot is non-linear and does not pass through the origin, indicating that film diffusion controls the phenol adsorption rate onto A-P and AS2-P [20]. On the other hand, the plot of B_t vs t during the phenol adsorption with AS1-P is linear and passes near the origin, which further indicates that the intraparticle diffusion is the rate-controlling step, in contrast to the Weber-Morris model, which indicates that the external diffusion dominates. However, in the case of the AS1-P composite, equilibrium was not achieved, and it is not possible to obtain any relevant data using the diffusion models.

Conclusions

In this work, the composites based on silica, alginate, and activated carbon obtained by pyrolysis of *S. cerevisiae* were, for the first time, used for efficient adsorption of phenol from aqueous solutions. The new composites are classified as porous materials, which allow easier and faster diffusion of phenol into the interior of the composite (sample AS2-P). The presence of silica in the composites resulted in mechanical stability (samples AS1-P and AS2-P). The microstructure of the silica-alginate-activated carbon composite was strongly influenced by the alginate-silica weight ratio, resulting in different phenol removal kinetics and saturation capacities. The optimal microstructure and composition of the composites for phenol removal were found for the AS2-P sample with a silica-alginate ratio of 1:2. The sample with a higher concentration of silica (sample AS1-P) adsorbed less phenol, and the process was slower compared to the sample with a lower concentration of silica (sample AS2-P). On the other hand, the leaching of organic matter from the AS1-P sample was lower compared to AS2-P. The utilization of an alginate-activated carbon composite or a silica-alginate-activated carbon composite (the latter with an alginate-silica weight ratio of 2:1) resulted in external diffusion limitations, while the utilization of a silica-alginate-activated carbon composite (the latter with an alginate-silica weight ratio of 1:1) resulted in intraparticle diffusion limitations.

Although in comparison with activated carbon, the removal efficiency of composites in phenol adsorption was slightly lower, this study could be significant as a way to more easily separate activated carbon-based adsorbents from aqueous solution with significant phenol removal efficiency, good mechanical stability, and minimal effect on the quality of treated water through secondary contamination by adsorbents. In general, composites based on silica-alginate and activated carbon can potentially be applied in real systems/bioreactors for pollutant removal, which requires further research in this field.

Acknowledgments

This work was financially supported by the Ministry of Science, Technological Development and Innovations of the Republic of Serbia, Project No. 451-03-136/2025-03/200088.

Conflict of Interest

The authors declare no conflict of interest.

References

1. RASHED M.N. Organic pollutants – monitoring, risk and treatment. 1st Edition, CroatiaEditor: M.Nageeb Rashed, Intech Publisher, **2013**.
2. GU H.M., BERGMAN R., ANDERSON N., ALANZA-ROSENBAUM S. Life cycle assessment of activated carbon from woody biomass. Wood and Fiber Science, **50** (3), 229, **2018**.
3. LABUTO G., CARVALHO A.P., MESTRE A.S., DOS SANTOS M.S., MODESTO H.R., DIAS MARTINS T., LEMOS S.G., DA SILVA H.D.T., CARRILHO E.N.V.M., CARVALHO W.A. Individual and competitive adsorption of ibuprofen and caffeine from primary sewage effluent by yeast-based activated carbon and magnetic carbon nanocomposite. Sustainable Chemistry and Pharmacy, **28**, 100703, **2022**.
4. WU G., JEONG T.-S., WON C.-H., LONGZHE CUI L. Production and characterization of activated carbon derived from brewer's yeast. Korean Journal of Chemical Engineering, **27** (5), 1476, **2010**.

5. MODESTO H.R., LEMOS S.G., DOS SANTOS M.S., KOMATSU J.S., GONÇALVES M., CARVALHO W.A, CARRILHO E.N.V.M., LABUTO G. Activated carbon production from industrial yeast residue to boost up circular bioecenomy. Environmental Science and Pollution Research, **28** (19), 24694, **2021**.
6. RAMOS J., MONTEIRO J.D.F., DOS SANTOS M.S., CARRILHO E.N.V.M. Sustainable alternative for removing pesticides in water: Nanomodified activated carbon produced from yeast residue biomass. Sustainable Chemistry and Pharmacy, **29**, 100794, **2022**.
7. ALAM S., ILYAS M., ULLAH S., RAHMAN N., ZAHOOR M., UMAR N.M., ULLAH R. Fabrication of magnetic activated carbon from corn-cob biomass for the removal of acidic dyes from waste water. Desalination and Water Treatment, **317**, 100049, **2024**.
8. ZHANG Y., ZHANG B.-T., TENG Y., ZHAO J. Activated carbon supported nanoscale zero valent iron for cooperative adsorption and persulfate-driven oxidation of ampicillin. Environmental Technology & Innovation, 19, 100956, 2020.
9. PERULLINI M., CALCABRINI M., JOBBÁGY M., BILMES S.A. Alginate/porous silica matrices for the encapsulation of living organisms: Tunable properties for biosensors, modular bioreactors, and bioremediation devices. Mesoporous Biomaterials, **2**, 3, **2015**.
10. MARTINS S.C.S., MARTINS C.M., FIÚZA L.M.C.G., SANTANELLA S.T. Immobilization of microbial cells: A promising tool for treatment of toxic pollutants in industrial wastewater. African Journal of Biotechnology, **12** (28), 4412, **2013**.
11. WANG B., WANC Y., ZHENG Y., LEE X., LIU T., YU Z., HUANGE J., OK Y.S., CHEN J., GAO B. Alginate-based composites for environmental applications: A critical review. Critical Reviews in Environmental Science and Technology, **49** (4), 318, **2019**.
12. IBANEZ J.P., UMETSU Y. Potential of protonated alginate beads for heavy metals uptake. Hydrometallurgy, **64** (2), 89, **2002**.
13. KIM T.Y., JIN H.J., PARK S.S., KIM S.J., CHO S.Y. Adsorption equilibrium of copper ion and phenol by powdered activated carbon, alginate bead and alginate-activated carbon bead. Journal of Industrial and Engineering Chemistry, **14** (6), 714, **2008**.
14. THAKUR S., PANDEY S., AROTIBA O.A. Development of a sodium alginate-based organic/inorganic super absorbent composite hydrogel for adsorption of methylene blue. Carbohydrate Polymers, **153**, 34, **2016**.
15. NAYL A.A., ABD-ELHAMIDM A.I., ALYL A.A., BRÄSE S. Recent progress in the applications of silica-based nanoparticles. RSC Advances, **12** (22), 13706, **2022**.
16. ALI E.M.A., SAYED M.A., ABDEL-RAHMAN T.M., HUSSEIN A.M., HUSSEIN R. Wastewater from cadmium pollution using silicon dioxide nanoparticles and fungal biomasses. Journal of Pure and Applied Microbiology, **13** (3), 1561, **2019**.
17. NIKOLIĆ M.P., FILIPOVIĆ R., STANOJEVIĆ-NIKOLIĆ S. Effect of reaction time on formation of silica core/shell particles. Processing and Application of Ceramics, **9** (4), 209, **2015**.
18. RAZAK N.A.A., OTHMAN N.H., SHAYUTI M.S.M., JUMAHAT A., SAPIAI N., LAU W.J. Agricultural and industrial waste –derived mesoporous silica nanoparticles: A review on chemical synthesis route. Journal of Environmental Chemical Engineering, **10** (2), 107322, **2022**.
19. GÜRCAN E.H., AKYOL R.B., CORUHS. Kinetic, isotherm modeling analyses of the adsorption of phenol on activated carbon/alginate composites. International Journal of Phytoremediation, **25** (7), 832, **2023**.
20. KHAN A.S., IBRAHIM T.H., KHAMIS M.I., NANCARROW P., IGBAL J., ALNASHEF I., JABBAR N.A., HASSAN N.F., MJALLI F.S. Preparation of sustainable activated carbon-alginate beads impregnated with ionic liquid for phenol decontamination. Journal of Cleaner Production, **321**, 128899, **2021**.
21. KHOJ A.M. Fabrication of silica/calcium alginate nanocomposite based on rice husk ash for efficient adsorption of phenol from water. RSC Advances, **14** (33), 24322, **2024**.
22. AGBALE N.R., AJIEH M.U., OGUNLEYE O.O., AGARRY S.E., ARINKOOLA A.O., OWEBOR K. Efficient simultaneous adsorptive removal of heavy metals and organics in produced water by a novel multi-functional alginate encapsulated kaolin -plantain pseudo-stem and snail shell composite biochar. NIPES Journal of Science and Technology Research, **7** (2), 383, **2025**.
23. CARABAJAL M., PERULLINI M.C.M., JOBBAGY M., ULLRICH R., LEVIN L. Removal of phenol by immobilization of *Tremetes versicolor* in silica-alginate-fungus biocomposites and loofa sponge. Clean-Soil, Air, Water, **44** (2), 180, **2016**.
24. SHIM J., LIM J-M, SHEA P.J., OH B-T. Simultaneous removal of phenol, Cu and Cd from water with corn cob silica-alginate beads. Journal of Hazardous Materials, **272**, 129, **2014**.
25. KUKIĆ V.D., ŠĆIBAN M., VASIĆ M.V., PRODANOVIĆ M.J. Secondary contamination of water during the biosorption of heavy metal ions pristine and sugar beet shreds from bioethanol production. Acta Periodica Technologica, **49**, 81, **2018**.
26. ŠĆIBAN M., KLAŠNJA M. Study of the adsorption of copper(II) ions from water onto wood sawdust, pulp and lignin. Adsorption Science and Technology, **22** (3), 195, **2004**.
27. PARK D., LIM S.-R., YUN Y.-S., PARK J.M. Development of a new Cr(VI)-biosorbent from agricultural biowaste. Bioresururce Technology, **99** (22), 8810, **2008**.
28. WU G., JEONG T.-S., WON C.-H., Cui L. Comparison of catalytic ozonation of phenol by activated carbon and manganese-supported activated carbon prepared from brewing yeast. Korean Journal of Chemical Engineering, **27** (1), 168, **2010**.
29. STANOJEVIĆ-NIKOLIĆ S., PAVLOVIĆ V.K., NIKOLIĆ P.M., SRDIĆ V.V., ŠĆIBAN M. Removal of cadmium(II) ions using *Saccharomyces cerevisiae* and *Leuconostoc mesenteroides* immobilized in silica materials by two processing methods. Materials Research, **25**, e20210568, **2022**.
30. DERAFA G., ZAGHOUANE-BOUDIAF H. New eco-friendly composite beads from biomass activated carbon for removal of highly toxic 2,4-dichlorophenol from aqueous medium: equilibrium, modeling and thermodynamic studies. Desalination and Water Treatment, **209**, 324, **2021**.
31. HO Y.S., MCKAY G. A comparasion of chemisorption kinetic models applied to pollutant removal on various sorbent. Process Safety and Environmental Protection, **76** (4), 332, **1998**.
32. WEBER W.J., MORRIS J.C. Kinetics of adsorption on carbon from solution. Journal of the Sanitary Engineering Division, **89** (2), 31, **1963**.

33. WANG J., GUO X. Adsorption kinetic models: Physical meanings, applications, and solving methods. Journal of Hazardous Materials, **390**, 122156, **2020**.
34. BOYD G.E., ADAMSON A.W., MEYERS L.S. The exchange adsorption of ions from aqueous solution by organic zeolites. II Kinetics. Journal of the American Chemical Society, **69** (11), 2836, **1947**.
35. REICHENBERG D. Properties of ion-exchange resins in relation to their structure. III. Kinetics of exchange. Journal of the American Chemical Society, **75** (3), 589, **1953**.
36. GAN Y.X. Activated carbon from biomass sustainable sources. C-Journal of Carbon Research, **7** (2), 39, **2021**.
37. CORTÈS-CAMARGO S., ROMÁN-GUERRERO A., ALVAREZ-RAMIREZ J., ALPIZAR-REYES E., VELAZQUEZ-GUTIÈRREZ S.K., PÈREZ-ALONSO C. Microstructural influence on physical properties and release profiles of sesame oi lencapsulated into sodium alginate-tamarind mucilage hydrogel beads. Carbohydrate Polymer Technologies and Applications, **5**, 100302, **2023**.
38. DAI F., ZHUANG Q., HUANG G., DENG H., ZHANG X. Infrared Spectrum Characteristics and Quantification of OH Groups in Coal. American Chemical Society Omega, **8** (19), 17064, **2023**.
39. BAKTI I.A., GARESO L.P. Characterization of active carbon prepared from coconuts shells using FTIR, XRD and SEM techniques. Jurnal Ilmiah Pendidikan Fisika Al-BiRuNi, **7** (1), 33, **2018**.
40. LIU J., LIU Y., PENG J., JIANG Y., MENG M., ZHANG W., NI L. Preparation of High Surface Area Oxidized Activated Carbon from Peanut Shell and Application for the Removal of Organic Pollutants and Heavy Metal Ions. Water Air and Soil Pollution, **229** (12), 391, **2018**.
41. NASTAJ J., PRZEWŁOCKA A., RAJKOWSKA-MYŚLIWIEC M. Biosorption of Ni(II), Pb(II) and Zn(II) on calcium alginate beads: equilibrium, kinetic and mechanism studies. Polish Journal of Chemical Technology, **18** (3), 81, **2016**.
42. LI K.-M., JIANG S.-C., CHEN X.-J., ZAN F. Influence of silica types on synthesis and performanceof amine-silica hybrid materials used for CO_2 capture. The Journal of Physical Chemistry C, **118** (5), 2454, **2014**.
43. D'ANGELO A., MORTALÓ C., COMUNE L., RAFFAINI G., FIORENTINO M., CATAURO M. Sol–Gel synthesized silica/sodium alginate hybrids: comprehensive physico-chemical and biological characterization. Molecules, **30** (17), 3481, **2025**.
44. YANG J., FU L., WU F., CHEN X., WU C., WANG Q. Recent developments in activated carbon catalysts based on pore size regulation in the application of catalytic ozonation. Catalysts, **12** (10), 1085, **2022**.
45. ESIFFI K., BRAHMI M., BOUSSETTA A., CHARII H., BENHAMOU A.A., BACHIRI A.E. Synergistic enhancement of chlorophenols removal using eco/friendly alginate@montmorillonite hybrid bio-capsules: insights from encapsulation and kinetic release studies. Journal of Microencapsulation, **41** (7), 601, **2024**.
46. RAMACHANDRAN S., CORADIN T., JAIN P.K., VERMA S.K. *Nostoc calcicola* immobilized in silica-coated calcium alginate and silica gel for applications in heavy metal biosorption. Silicon, **1**, 215, **2009**.
47. LORENC-GRABOWSKA E. Effect of micropore size distribution on phenol adsorption on steam activated carbons. Adsorption, **22**, 599, **2016**.
48. COLEMAN N.T., McCLUNG A.C., MOORE D.P. Formation constants Cu(II)-peat complexes. Science, **123** (3191), 330, **1956**.